RSC Advances

PAPER

View Article Online
View Journal | View Issue

Cite this: *RSC Adv.*, 2021, **11**, 29441

New pyridine and chromene scaffolds as potent vasorelaxant and anticancer agents†

Dina H. Dawood,[a] Aladdin M. Srour,[*b] Dalia O. Saleh,[c] Kelley J. Huff,[d] Francesca Greco[d] and Helen M. I. Osborn[d]

Based on studies that have reported the association between cancer and cardiovascular diseases, new series of pyridine- (**3a–o**) and/or chromene- (**4a–e**) carbonitrile analogous were designed, synthesized and screened for their vasodilation and cytotoxic properties. The majority of the new chemical entities demonstrated significant vasodilation efficacies, compounds **3a**, **3h**, **3j**, **3m**, **3o**, **4d** and **4e** exhibited the most promising potency with IC_{50} = 437.9, 481.0, 484.5, 444.8, 312.1, 427.6 and 417.2 μM, respectively, exceeding prazosin hydrochloride (IC_{50} = 487.3 μM). Compounds **3b–e**, **3k** and **3l** also, revealed moderate vasodilation activity with IC_{50} values ranging from 489.7 to 584.5 μM. In addition, the anti-proliferative activity evaluation of the experimental compounds at 10 μM on the MCF-7 and MDA-MB 231 breast cancer cell lines illustrated the excellent anti-proliferative properties of derivatives **3d**, **3g** and **3i**. Compound **3d** was the most potent analogue with IC_{50} = 4.55 ± 0.88 and 9.87 ± 0.89 μM against MCF-7 and MDA-MB 231, respectively. Moreover, compound **3d** stimulated apoptosis and cell cycle arrest at the S phase in MCF-7 cells in addition to its capability in accumulation of cells in pre-G1 phase and activating caspase-3. Furthermore, the molecular docking of **3d** was performed to discover the binding modes within the active site of caspase-3. **3d**, as the only common bi-functional agent among the tested hits, demonstrated that new pyridine-3-carbonitrile derivatives bearing cycloheptyl ring systems offer potential as new therapeutic candidates with combined vasodilation and anticancer properties.

Received 19th June 2021
Accepted 23rd August 2021

DOI: 10.1039/d1ra04758b

rsc.li/rsc-advances

1. Introduction

Two major leading causes of mortality worldwide are cardiovascular disturbances and cancer. For example, hypertension is one of the main causes of diseases that lead to human angiocardiopathy death.[1] Currently, based on statistics from the World Health Organization, 1.13 billion people worldwide are diagnosed with hypertension (WHO, 2020)[2] which can contribute to the development of diabetes, renal failure, and heart diseases.[2,3] Also, cancer was responsible for 10 million deaths in 2020 and despite the vast leap in cancer therapy, one from six deaths is due to cancer.[4]

Interestingly, multiple studies have recently hypothesized an association between hypertension, and cancer incidence and cancer mortality.[5–8] For example, an epidemiological survey revealed that patients with cardiovascular disease have higher risks of developing cancer compared with the other population. Moreover, a meta-analysis of 13 prospective studies demonstrated that elevated blood pressure was related to a 7% higher breast cancer risk.[9,10] As both diseases share common risk factors such as obesity, diabetes mellitus and alcoholism, this may clarify their synchronous occurrence.[11] Indeed, this association termed as reverse cardio-oncology (cancer risk in patients with cardiovascular disease) is now an area of focus for both clinicians and basic scientists.[12] Of particular relevance to our work is emerging evidence that cancer and cardiovascular diseases might share some biological pathways.[5] However, to date, only few studies have focused on developing therapeutic agents that may offer dual potential for treating both cardiovascular disease and cancer, and hence addressing the therapeutic challenges of treating reverse cardio-oncology. Within this programme, we therefore aimed to identify, design and develop appropriate small molecules containing pharmacophores of potential interest for the treatment of cardiovascular disease and cancer, and hence for reverse cardio-oncology. At the same time, challenges associated with treating the individual diseases would also be addressed by identifying new lead compounds for development for application for each condition.

[a]*Chemistry of Natural and Microbial Products Department, Pharmaceutical and Drug Industries Research Division, National Research Centre, 33 El Bohouth St., Dokki, Giza 12622, Egypt*

[b]*Department of Therapeutic Chemistry, National Research Centre, 33 El Bohouth St., Dokki, Giza 12622, Egypt. E-mail: alddinsrour@gmail.com*

[c]*Pharmacology Department, National Research Centre, 33 El Bohouth St., Dokki, Giza 12622, Egypt*

[d]*School of Pharmacy, University of Reading, Whiteknights, Reading, RG6 6AD, UK*

† Electronic supplementary information (ESI) available. See DOI: 10.1039/d1ra04758b

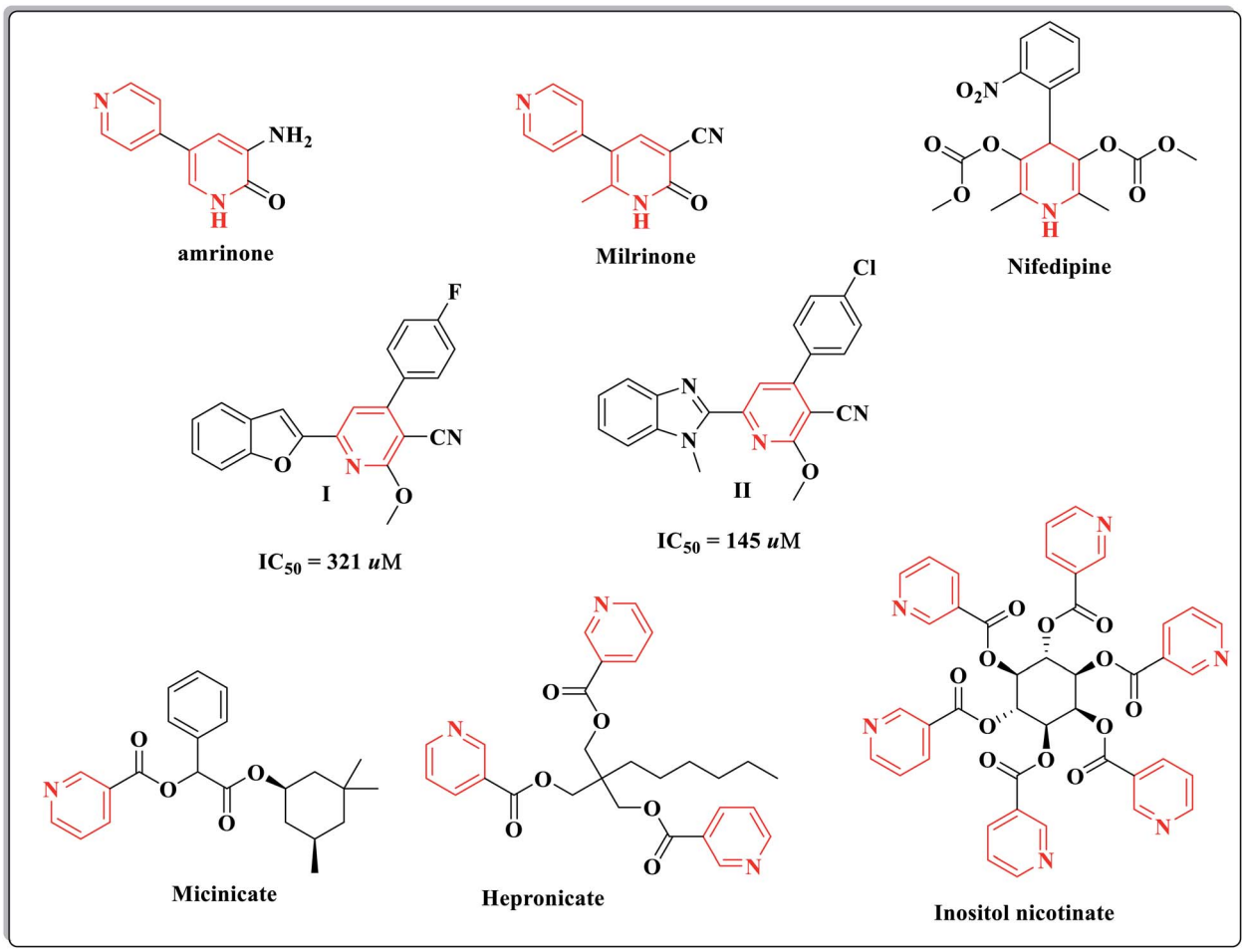

Fig. 1 Different pyridine-based derivatives of potent vasodilation activity.

Numerous antihypertensive candidates have been developed to control high blood pressure such as potassium channel activators, calcium channel blockers, and angiotensin-converting enzyme inhibitors (ACEI). However, despite the progress in the newly developed targeted therapies, these treatment strategies mainly depend on vasodilation to reduce blood pressure.[13] As a result, the drawbacks on systemic hypotension and limited efficiency are still challenging clinical problems, leading to poor prognosis.[14] Thus, new antihypertensive therapeutics acting on a range of therapeutic targets are urgently needed to control hypertension more effectively and minimize adverse side-effects that are often associated with conventional agents.

A literature survey has reported that many pyridine derivatives play a vital role in vasorelaxation therapeutics.[15] For example, milrinone and amrinone are positive inotropic agents with vasodilator properties; nifedipine is a peripheral and coronary vasodilator drug of the calcium channel blockers.[15–17] Furthermore, different pyridine-3-carbonitrile analogs **I**, **II** and different nicotinate esters such as micinicate, hepronicate and inositol nicotinate have emerged as significant vasodilating agents (Fig. 1).[18–22]

Oxygen heterocyclic compounds are frequently developed as potential therapeutic targets by medicinal chemists owing to their relatively low inherent toxicity.[23] For example, different pyrano analogues such as compounds **III**, **IV** [24–27] as well as structural hybridization of scopoletin, a benzopyran-2-one derivative, with a benzopyran (chromene) nucleus, have led to the formation of substituted chromeno-coumarin hybrids of effective vasorelaxant activity. Moreover, glabridin bearing pyranobenzopyran core is a known vasorelaxing agent[23] (Fig. 2).

In addition to their previously displayed vasodilation properties, pyridine- and/or chromene-based heterocycles have also demonstrated anticancer properties and potential as apoptotic inducers through caspase-3 activation[28–32] (Fig. 3).

Encouraged by the observed effective vasorelaxant and anticancer activities of various analogues bearing pyridine as well as pyran and chromene rings, novel 2-methoxy-pyridine-3-carbonitriles and/or 2-aminopyran ring systems bearing various aromatic or heterocyclic moieties at C-4 and fused with different cycloalkane ring systems were identified for exploration in this study. The new chemical entities **3a–o** and **4a–e** were therefore identified as targets of interest herein for their potential as new and effective candidates for reverse cardio-oncology due to their dual vasodilation and anticancer functions.

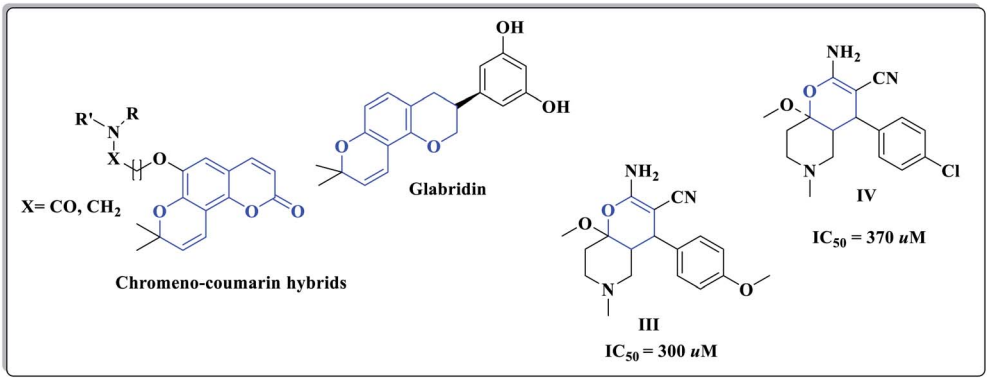

Fig. 2 Various pyrano and chromeno derivatives of potent vasodilation activity.

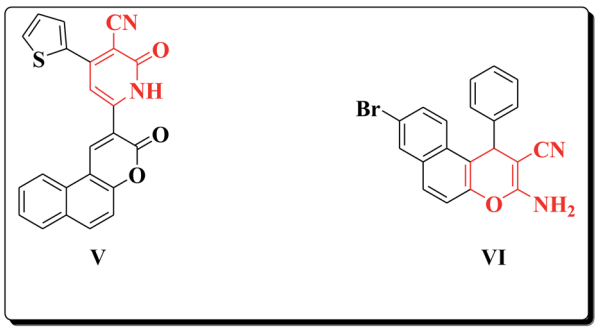

Fig. 3 Pyridine and chromene based compounds as anticancer agents.

2. Results and discussion

2.1. Chemistry

The reaction of ylidenemalononitriles **2a–m** with cyclohexanone and/or cycloheptanone in the presence of sodium methoxide was utilized to accomplish a regioselective Michael addition reaction of the active methylene of 4-cycloalkanone at the β-carbon of arylidinemalononitriles **2a–m**. The latter derivatives underwent subsequent cyclization (due to the methoxide attack at one of the nitrile groups), dehydration and then dehydrogenation to afford the corresponding *2-methoxy-4-aryl-6,7-dihydro-5H-cycloalkyl[b]pyridine-3-carbonitrile* derivatives (**3a–o**). An alternative pathway has also been hypothesized to occur through a nucleophilic attack of the active methylene of cyclohexanone at the β-carbon of the unsaturated dinitrile function in the presence of the basic catalyst. Cyclization occurred as a result of the methoxide nucleophilic attack at 4-cyclohexanone carbonyl function, followed by interaction with the neighboring nitrile group.[33] In this way, the corresponding *2-amino-4-(4-aryl)-8a-methoxy-4a,5,6,7,8,8a-hexahydro-4H-chromene-3-carbonitrile* analogs (**4a–e**) were also afforded for analysis, as shown in Scheme 1.

The derivatives (**3a–o**) and (**4a–e**) were characterized using a range of spectroscopic methods. For instance, compound **3a** which is a representative member of the *pyridine-3-carbonitrile* series **3a–o**, showed a strong stretching IR band at ν = 2220 cm^{-1} for (C≡N) with no detection of the band representative of the carbonyl stretching vibration. The ^{1}H-NMR spectrum also indicated the methylene protons H_2C-6, H_2C-7 and H_2C-8 as multiplet at δ_H = 1.49–1.87 ppm while H_2C-5 and H_2C-9 were present as two triplets at δ_H = 2.53 and 3.04 ppm, respectively. The methoxy signal was resonating at δ_H = 4.05 ppm. The ^{13}C-NMR spectrum for compound **3a** showed the pyridinyl *C-3* at δ_C = 93.73 ppm as well as the methoxy and nitrile carbons at δ_C = 54.13 and 115.57, respectively. EI mass spectrometric analysis demonstrated the parent ion peak *m*/*z* (%) 278 (M^+, 66), 277 (100).

Considering compound **4a** as a representative example for the *chromene-3-carbonitrile* analogs **4a–e**, strong stretching vibrational bands were evident at ν = 3449, 3348 cm^{-1} for (NH_2), and at ν = 2187 cm^{-1} for (C≡N). Moreover, the ^{1}H-NMR spectrum revealed the methoxy group at δ_H = 3.32 ppm, while the characteristic NH_2 protons were assigned at δ_H = 4.36 ppm, the methylene functions H_2C-5, H_2C-6, H_2C-7 and H_2C-8 were resonating at δ_H = 1.07–1.87 ppm, as well as the methine protons *HC-4a* and *HC-4* were observed as a multiplet at δ_H = 2.30–2.39 ppm and a broad singlet at δ_H = 3.29 ppm, respectively. The ^{13}C-NMR spectrum for the same compound revealed the methylene carbons H_2C-5, H_2C-6, H_2C-7 and H_2C-8 at δ_C = 22.34, 25.06, 26.50, 30.86 ppm, respectively, the methine carbons *HC-4* and *HC-4a* were detected at δ_C = 40.80 and 47.13 ppm, respectively. Also, the methoxy and the nitrile carbons were detected at δ_C = 48.65 and δ_C = 120.81 ppm, respectively, along with the characteristic quaternary carbon *C-8a* at δ_C = 102.76 ppm. EI mass spectrometric analysis revealed the relative intensity value of the parent ion peak *m*/*z* (%) 284 (M, 4.6), 112 (100). The established chemical structures of all of the new chemical entities were proven *via* spectral data (IR, ^{1}H NMR, ^{13}C NMR, MS) and exhibited similar features to those discussed for **3a** and **4a** (*cf.* Experimental section), the spectral charts (IR, ^{1}H-, ^{13}C-NMR and MS) of the new synthesized compounds are available in the ESI (Fig. S1–S79†).

2.2. Biological activity

2.2.1. Vasodilation properties. The novel substituted pyridine-/chromene-carbonitriles **3a–o** and **4a–e**, respectively, were tested for their vasodilation properties following a well-

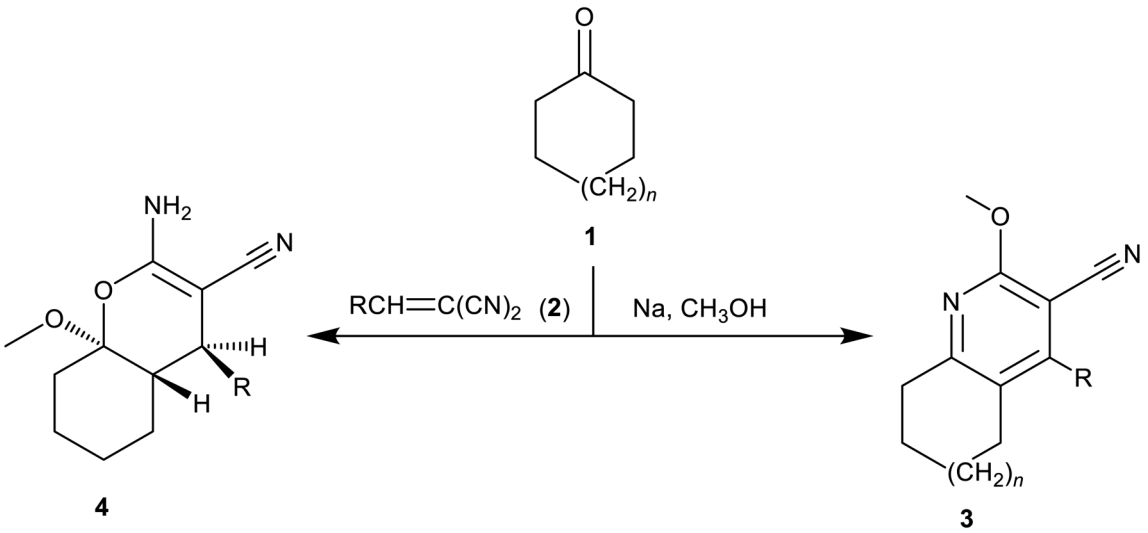

1a; $n = 1$
1b; $n = 2$
2a; R = C_6H_5
2b; R = 4-$H_3CC_6H_4$
2c; R = 3-$H_3COC_6H_4$
2d; R = 4-$H_3COC_6H_4$
2e; R = 4-FC_6H_4
2f; R = 3-ClC_6H_4
2g; R= 4-ClC_6H_4
2h; R= 3-BrC_6H_4
2i; R = 4-BrC_6H_4
2j; R = 3-Indolyl
2k; R = N-Methyl-3-indolyl
2l; R = N-Ethyl-3-indolyl
2m; R = 2-Napthyl

3a; R = C_6H_5, $n = 2$
3b; R = 4-$H_3CC_6H_4$, $n = 2$
3c; R = 3-$H_3COC_6H_4$, n = 2
3d; R = 4-$H_3COC_6H_4$, $n = 2$
3e; R = 4-FC_6H_4, $n = 2$
3f; R = 3-ClC_6H_4, $n = 2$
3g; R = 4-ClC_6H_4, $n = 2$
3h; R = 3-BrC_6H_4, $n = 2$
3i; R = 4-BrC_6H_4, $n = 2$
3j; R = 3-Indolyl, $n = 2$
3k; R = N-Methyl-3-indolyl, $n = 1$
3l; R = N-Methyl-3-indolyl, $n = 2$
3m; R = N-Ethyl-3-indolyl, $n = 1$
3n; R = N-Ethyl-3-indolyl, $n = 2$
3o; R = 2-Naphthyl, $n = 2$
4a; R = C_6H_5
4b; R = 4-$H_3CC_6H_4$
4c; R = 4-$H_3COC_6H_4$
4d; R = 4-FC_6H_4
4e; R = 4-BrC_6H_4

Scheme 1 Synthetic routes for accessing the synthesized fused cycloalkane-pyridine-3-carbonitrile scaffolds **3a–o** and **4a–e**.

documented procedure using isolated thoracic aortic rings of mice pre-contracted with norepinephrine HCl. Prazosin hydrochloride was also included as a standard drug for comparison purposes. The observed results are displayed as IC_{50} values (Table 1) and dose response curves (Table S1 of ESI†). The obtained data shows that compounds **3a**, **3h**, **3j**, **3m**, **3o**, **4d** and **4e** represented notable vasodilation efficiency with IC_{50} = 437.9, 481.0, 484.5, 444.8, 312.1, 427.6 and 417.2 μM, respectively, exceeding that of prazosin hydrochloride (IC_{50} = 487.3 μM). However, the tested analogous **3b–e**, **3k** and **3l** exhibited modest vasodilation activity with IC_{50} values extent from 489.7 to 584.5 μM. On the other hand, derivatives **3f–g**, **3i**, **3n** and **4a–c** revealed weak vasodilation activity with IC_{50} range lies from 608.6 to 758.6 μM. It is obvious that the vasodilation activity is enhanced when cycloheptapyridine-3-carbonitrile scaffold is attached with 2-napthyl more than phenyl, substituted phenyl and/or 3-indolyl rings as shown in **3o**, **3a**, **3b**, **3h** and **3j**, respectively. Likewise, the conjugation of chromene-3-carbonitrile group with phenyl rings of electron withdrawing substituents resulted in significant vasodilation efficiency as **4d** and **4e**. Thus the cycloalkane-pyridine-3-carbonitrile scaffolds incorporated with substituted aryl and/or heterocyclic rings might be developed into potent vasodilation candidates.

Table 1 Vasodilatory activity (IC_{50} μM) in rat thoracic aortic rings

Entry	Compound	R	*n*	Potency IC_{50} μM ± SD[a]	SEM ($n = 6$)
1	**3a**	C_6H_5	2	437.9 ± 8.57	3.50
2	**3b**	4-$H_3CC_6H_4$	2	489.7 ± 9.67	3.95
3	**3c**	3-$H_3COC_6H_4$	2	532.8 ± 10.45	4.27
4	**3d**	4-$H_3COC_6H_4$	2	524.1 ± 8.25	3.37
5	**3e**	4-FC_6H_4	2	558.6 ± 12.88	5.26
6	**3f**	3-ClC_6H_4	2	608.6 ± 16.65	6.80
7	**3g**	4-ClC_6H_4	2	698.3 ± 11.65	4.75
8	**3h**	3-BrC_6H_4	2	481.0 ± 13.39	5.47
9	**3i**	4-BrC_6H_4	2	758.6 ± 13.00	5.31
10	**3j**	3-Indolyl	2	484.5 ± 15.02	6.13
11	**3k**	*N*-Methyl-3-indolyl	1	584.5 ± 12.70	5.19
12	**3l**	*N*-Methyl-3-indolyl	2	558.6 ± 11.20	4.57
13	**3m**	*N*-Ethyl-3-indolyl	1	444.8 ± 13.79	5.63
14	**3n**	*N*-Ethyl-3-indolyl	2	739.7 ± 11.67	4.76
15	**3o**	2-Naphthyl	2	312.1 ± 9.05	3.70
16	**4a**	C_6H_5	1	710.2 ± 12.02	4.91
17	**4b**	4-$H_3CC_6H_4$	1	674.1 ± 11.57	4.72
18	**4c**	4-$H_3COC_6H_4$	1	639.7 ± 10.55	4.31
19	**4d**	4-FC_6H_4	1	427.6 ± 8.26	3.37
20	**4e**	4-BrC_6H_4	1	417.2 ± 9.35	3.82
21	Prazosin HCl		—	487.3 ± 10.13	4.14

[a] SD = standard deviation.

2.2.2. Cytotoxic data of experimental compounds against cancer cells. The experimental compounds were also screened for their anti-proliferative activity at 10 μM against the MCF-7 and MDA-MB 231 breast cancer cell lines using the MTT assay. The results shown in Fig. 4 and 5 illustrate that whilst the majority of compounds appeared to have little to no effect on cell viability at this concentration, others such as **3d**, **3g** and **3i** exhibited relatively good cytotoxic activity, with inhibition percentage around 50–60%. After initial screening, it was clearly noticed that the investigated derivatives demonstrated higher cytotoxic efficiency towards the MCF-7 cell line than the MDA-MB 231 cells. For example, compounds **3d**, **3g** and **3i** revealed excellent cytotoxic efficiency against the MCF-7 cell line, with compound **3d** being the most effective against the MDA-MB 231 cell line. The most active derivatives were selected for further study, in order to determine their IC_{50} values. As depicted in Table 2, compound **3d** showed excellent cytotoxic efficacy on MCF-7 with $IC_{50} = 4.55 \pm 0.88$ μM which illustrates greater activity than 5-fluouracil which is drug often used in chemotherapy regimens for breast cancer ($IC_{50} = 7.10 \pm 0.90$ μM). Furthermore, compounds **3g** and **3i** also exhibited promising efficiency with $IC_{50} = 11.52 \pm 2.60$ and 11.23 ± 3.27 μM, respectively. Moreover, compound **3d** showed remarkable cytotoxic efficiency against MDA-MB 231 cells with $IC_{50} = 9.87 \pm 0.89$ μM exceeding that of 5-fluouracil ($IC_{50} = 15.10 \pm 0.90$ μM). It is noteworthy that compound **3d** displayed significant activity against each of the two breast cancer cell lines. Hence, it was concluded that the inclusion of 4-methoxy-phenyl with cycloheptapyridine-3-carbonitrile fused system was beneficial for the cytotoxic efficiency against both types of breast cancer cell lines (Fig. 2 and 3 in ESI†). Alternatively, compounds **3d**, **3g**

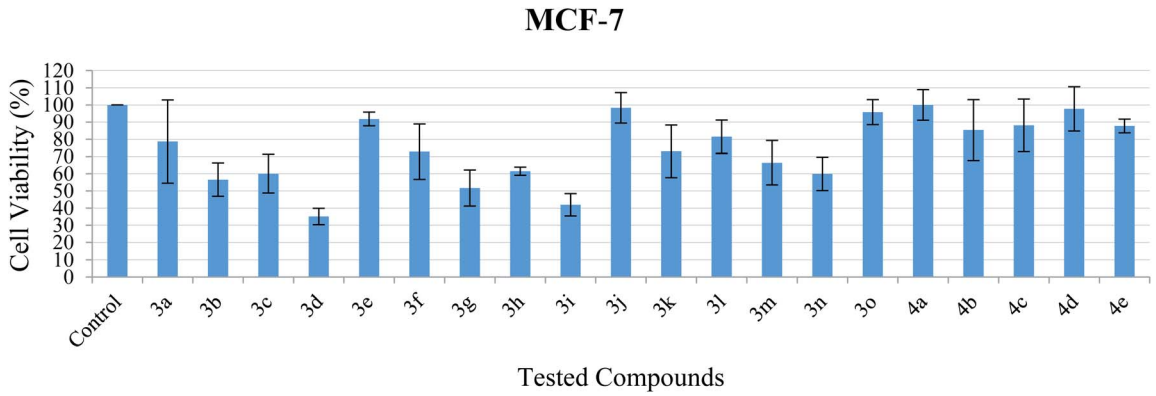

Fig. 4 Cell viability of MCF-7 after exposure to the compounds at 10 μM. Data indicate mean ± SEM, $n \geq 3$.

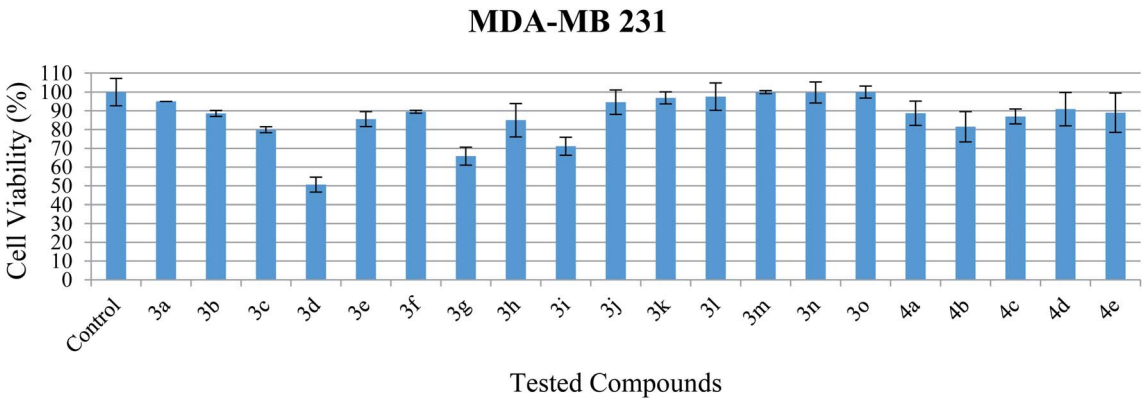

Fig. 5 Cell viability of MDA-MB 231 after exposure to the compounds at 10 μM. Data indicate mean ± SEM, $n \geq 3$.

Table 2 IC_{50} of tested compounds on MCF-7 and MDA-MB 231 cell lines, Data indicate mean IC_{50} ± SEM

Compound	MCF-7, IC_{50} (μM)	MDA-MB 231, IC_{50} (μM)
3d	4.55 ± 0.88	9.87 ± 0.89
3g	11.52 ± 2.60	—
3i	11.23 ± 3.27	—
5-FU	7.10 ± 0.90	15.10 ± 0.90

and **3i** represented moderate vasodilation activity. More structural optimization is needed to reach to new candidates possessing dual vasodilation and anticancer activities.

2.2.3. Cellular mechanism of action

2.2.3.1. Cell cycle arrest. Based on the prominent cytotoxic efficacy of compound **3d**, it was elected for more in-depth investigation to study its influence on the cell cycle development and apoptosis induction in MCF-7 cells. Flow cytometry data revealed that subjecting MCF-7 cells to compound **3d** at 4.55 μM for 24 h resulted in disruption of the normal cell cycle development. It was noticed that compound **3d** caused a remarkable increment in the percentage of cells at the pre-G1 phase from 1.74 to 26.97% in addition to an increase in the cell percentages at the S phase from 39.27 to 49.33%. On the other hand, a reduction in cell percentages at the G1 phase (from 52.35 to 42.71%) and the G2-M phase (from 8.38 to 7.96%) were observed compared to the untreated MCF-7 cells (Fig. 6), Therefore, it could be hypothesized that compound **3d** may suppress the proliferation of MCF-7 cells *via* induction of pre-G1 apoptosis and cell growth arrest at S phase.

2.2.3.2. Detection of apoptosis via annexin-V-FITC assay. Annexin V-FITC/propidium iodide (PI) dual staining of MCF-7 cells was also performed to assure and quantify the apoptosis percentage prompted by compound **3d**. A significant increase of apoptotic cells (late apoptosis) was detected upon treatment of MCF-7 cells with compound **3d** from 0.22 to 13.73%, additionally, considerable increase in the early apoptosis was noticed from 0.57 to 3.89% compared to the untreated MCF-7 cells. Furthermore, there was a pronounced increment of the percentage of necrotic cells from 0.95 to 9.35% (Fig. 7). Thus the anti-proliferative activity of compound **3d** was exerted *via* induction of apoptosis and necrosis.

2.2.3.3. Upregulation of caspase-3. It has been reported that caspase cascade events are essential mediators in the initiation of apoptosis through intrinsic or extrinsic pathways.[34,35] Therefore, the activation of caspase 3 has a crucial role in apoptotic cell death.[36] A significant increase by 3.77 fold was noticed in the induction of caspase-3 upon treating of MCF-7

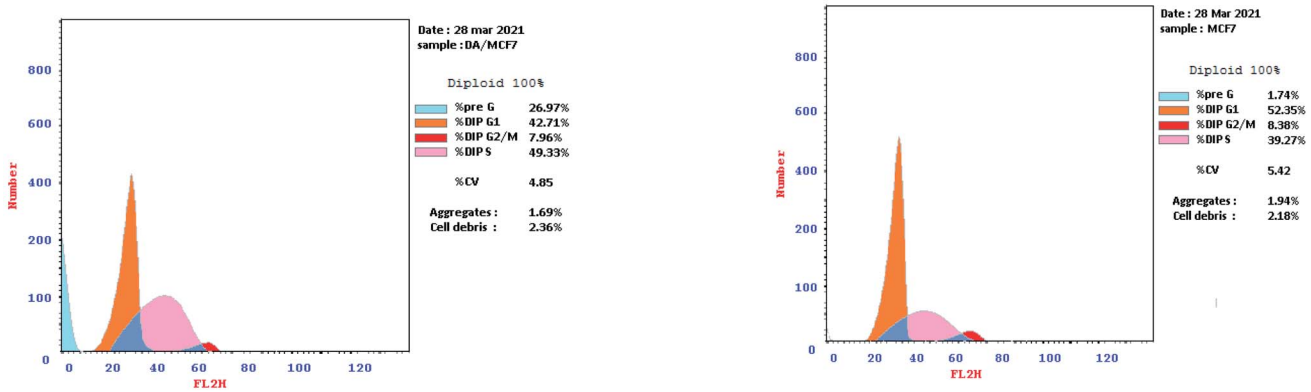

Fig. 6 The impact of compound **3d** on cell cycle progression of MCF-7 cells.

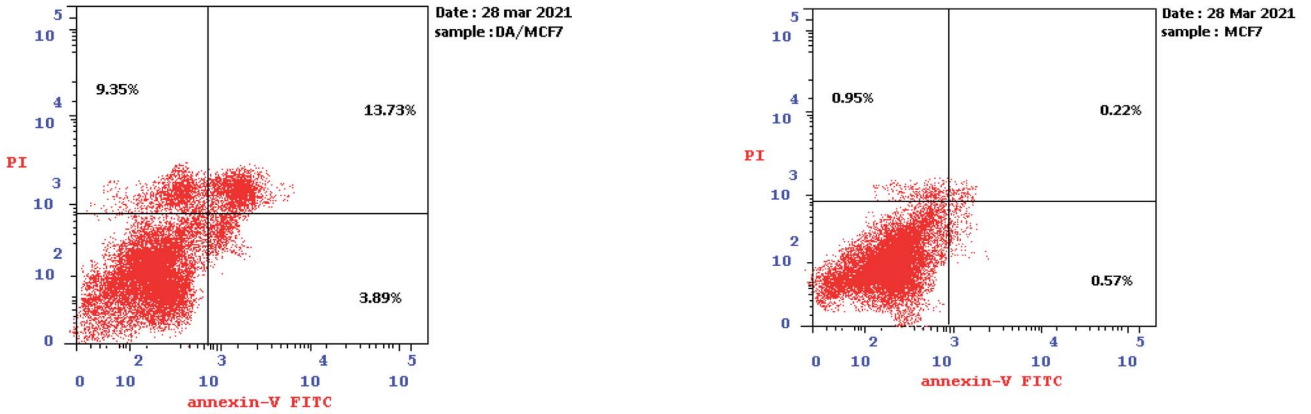

Fig. 7 The influence of compound **3d** in induction of apoptosis/necrosis of MCF-7 cells.

Table 3 The influence of compound **3d** on caspase-3 activity in MCF-7 cells

Compound	Conc. (μM)	RT-PCR, caspase-3, FLD
3d	4.55	3.77
Cont. MCF-7	—	1

cells with compound **3d** relative to the untreated MCF-7 cells (Table 3). Accordingly, it is hypothesized that the apoptotic process might be stimulated *via* activation of caspase-3.

3. Molecular docking study on caspase-3

The above results illustrate the significant apoptotic activity of the target compound **3d** that could be a result of activation of caspase-3. This was further probed through a molecular docking approach within the active binding site of caspase-3 kinase using Molecular Operating Environment (MOE-Dock) software version 2014.0901.[37,38] Firstly, the crystal structure of the key enzyme caspase-3 (PDB code: 2J30)[39] was retrieved from the RCSB Protein Data Bank and prepared for the docking process.

Docking of the promising activator **3d** gave a perfect energy score −12.40 kcal mol^{-1} as illustrated in Fig. 8. The nitrogen of the cyano group formed H-bond acceptors with the sidechains of the key amino acids **Arg64** and **His121** (distance: 3.20 and 2.52 Å, respectively). Furthermore, the centroid of the pyridine scaffold linked to **Arg207** through an arene–cation interaction. Interestingly, the cyclohepta[*b*]pyridine core fitted well within the binding site through hydrophobic interactions with the essential amino acids **Tyr204**, **Ser205**, **Trp206**, **Ser120**, **Gln161**, **Cys163** and **Phe256**.

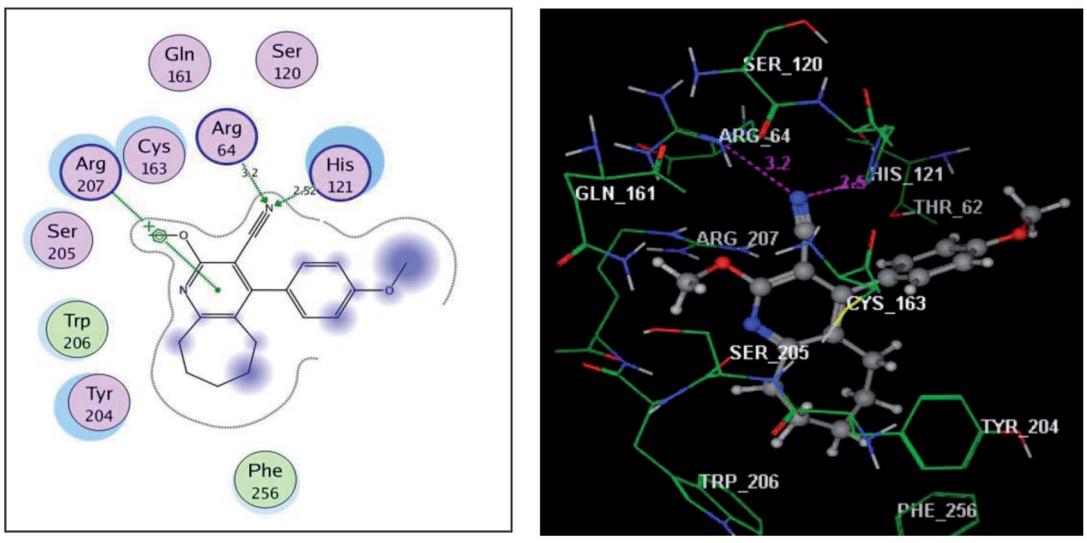

Fig. 8 (A) & (B) diagrams illustrate 2D and 3D binding modes of the new derivative, **3d** within the active site of caspase-3 (PDB: 2J30).

4. Conclusion

In this programme, we aimed to identify novel molecules with dual vasodilation and anti-cancer properties, in order to develop new opportunities for treating cardiovascular disease, cancer and reverse cardio-oncology. Reaction of ylidenemalononitriles **2a–m** with cyclohexanone and/or cycloheptanone in the presence of sodium methoxide was carried out regioselectively due to a Michael addition reaction to afford the corresponding pyridine- (**3a–o**) and chromene- (**4a–e**) carbonitrile analogous, respectively. The new chemical entities were scanned for their vasodilation and cytotoxic properties. The majority of the tested analogous revealed significant vasodilation efficacy, compound **3o** in particular was the most potent among the examined series with IC_{50} = 312.1 μM, which is superior to prazosin hydrochloride (IC_{50} = 487.3 μM). In addition, the antiproliferative results at 10 μM on MCF-7 and MDA-MB 231 breast cancer cell lines, indicated excellent activity of the derivatives **3d**, **3g** and **3i**. Compound **3d** was the most active against the MCF-7 and MDA-MB 231 cell lines with $IC_{50} = 4.55 \pm 0.88$ and 9.87 ± 0.89 μM, respectively. Furthermore, flow cytometry data revealed that compound **3d** stimulated apoptosis of MCF-7 cancer cells *via* activation of caspase-3 and arrested the cell cycle at the S phase along with its ability in accumulation of cells at the pre-G1 phase. Moreover, molecular docking for compound **3d** identified the interactions with key amino acids within the active binding site of caspase-3. Interestingly **3d** exhibited both vasodilation and anti-proliferative activities, demonstrating that pyridine-3-carbonitrile scaffolds bearing cycloheptyl ring systems are important functionalized precursors for further development of new vasodilation and anti-cancer dual active hits.

5. Experimental

5.1. Chemistry

Melting points were recorded on a Stuart SMP30 melting point apparatus. IR spectra (KBr) were recorded on a JASCO 6100 spectrophotometer. NMR spectra were recorded on a JEOL AS 500 (^{1}H: 500 MHz, ^{13}C: 125 MHz) and a BRUKER 400 (^{1}H: 400, ^{13}C: 100 MHz) spectrometers. Mass spectra were recorded on a Shimadzu GCMS-QP 1000 EX (EI, 70 eV) spectrometer, Elemental microanalyses were recorded on a Vario El Elementar analyzer, ylidenemalononitrile **2a–m** were prepared according to previously reported procedure.[19–21]

5.1.1. General procedure for synthesis of compounds. A mixture of equimolar amounts of **1a**,**b** and the corresponding ylidenemalononitrile **2a–m** (10 mmol) in methanol (25 mL) containing sodium (0.46 g, 20 mmol) was stirred at room temperature (20–25 °C) for 24 h. The separated solid was collected, washed with water and crystallized from an appropriate solvent affording **3a–o** and/or **4a–e**.

*5.1.1.1. 2-Methoxy-4-phenyl-6,7,8,9-tetrahydro-5H-cyclohepta [b]pyridine-3-carbonitrile (**3a**).* Colorless microcrystals from DMF; yield 1.65 g (59%); mp 214–215 °C; IR: ν_{max}/cm^{-1} 2220 (C≡N), 1558 (C=N). ^{1}H-NMR (400 MHz, $CDCl_3$): δ 1.49–1.87 (m, 6H), 2.53 (t, J = 5.4, 2H), 3.04 (t, J = 5.4, 2H), 4.05 (s, 3H), 7.21–7.26 (m, 2H), 7.40–7.49 (m, 3H). ^{13}C-NMR (100 MHz, $CDCl_3$): δ 26.07, 27.63, 29.07, 32.07, 39.57, 54.13, 93.73, 115.57, 128.42, 128.62, 128.76, 129.23, 136.36, 154.97, 161.99, 166.60. MS: *m*/*z* (%) 278.09 (M^+, 66), 277.03 (100). Anal. calcd for $C_{18}H_{18}N_2O$ (278.35): C, 77.67; H, 6.52; N, 10.06. Found: C, 77.80; H, 6.63; N, 10.16.

*5.1.1.2. 2-Methoxy-4-p-tolyl-6,7,8,9-tetrahydro-5H-cyclohepta [b]pyridine-3-carbonitrile (**3b**).* Colorless microcrystals from *n*-butanol; yield 1.67 g (57%); mp 228–230 °C; IR: ν_{max}/cm^{-1} 2221 (C≡N), 1587 (C=N). ^{1}H-NMR (400 MHz, $CDCl_3$): δ 1.49–1.87 (m, 6H), 2.42 (s, 3H), 2.55 (t, J = 5.6, 2H), 3.03 (t, J = 5.4, 2H), 4.04 (s, 3H), 7.10 (d, J = 8 Hz, 2H), 7.26 (d, J = 8.8 Hz, 2H). ^{13}C-NMR (100 MHz, $CDCl_3$): δ 21.32, 26.09, 27.65, 29.05, 32.09, 39.57, 54.08, 93.83, 115.76, 128.35, 129.29, 129.30, 133.38, 138.65, 155.15, 162.00, 166.47. MS: *m*/*z* (%) 292.10 (M^+, 75), 290.87 (100). Anal. calcd for $C_{19}H_{20}N_2O$ (292.37): C, 78.05; H, 6.89; N, 9.58. Found: C, 78.17; H, 6.93; N, 9.70.

*5.1.1.3. 2-Methoxy-4-(3-methoxy-phenyl)-6,7,8,9-tetrahydro-5H-cyclohepta[b]pyridine-3-carbonitrile (**3c**).* Pale yellow microcrystals from *n*-butanol; yield 1.82 g (59%); mp 171–172 °C; IR: ν_{max}/cm^{-1} 2219 (C≡N), 1635 (C=N). ^{1}H-NMR (400 MHz, $CDCl_3$): δ 1.49–1.87 (m, 6H), 2.53 (t, J = 5.2 Hz, 2H), 3.02 (t, J = 5.8 Hz, 2H), 3.86 (s, 3H), 4.05 (s, 3H), 6.73–6.80 (m, 2H), 6.96 (d, J = 10.8 Hz, 1H), 7.36 (t, J = 8 Hz, 1H). ^{13}C-NMR (100 MHz, $CDCl_3$): δ 26.07, 27.66, 29.10, 32.07, 39.55, 54.13, 55.30, 93.65, 114.08, 114.30, 115.50, 120.71, 129.19, 129.79, 137.61, 154.79, 159.53, 161.96, 166.58. MS: *m*/*z* (%) 308.08 (M^+, 100). Anal. calcd for $C_{19}H_{20}N_2O_2$ (308.37): C, 74.00; H, 6.54; N, 9.08. Found: C, 74.24; H, 6.40; N, 8.90.

*5.1.1.4. 2-Methoxy-4-(4-methoxy-phenyl)-6,7,8,9-tetrahydro-5H-cyclohepta[b]pyridine-3-carbonitrile (**3d**).* Colorless microcrystals from ethanol; yield 1.92 g (62%); mp 167–168 °C; IR: ν_{max}/cm^{-1} 2217 (C≡N), 1608 (C=N). ^{1}H-NMR (400 MHz, $CDCl_3$): δ 1.50–1.87 (m, 6H), 2.56 (t, J = 5.4 Hz, 2H), 3.03 (t, J = 5.6 Hz, 2H), 3.85 (s, 3H), 4.04 (s, 3H), 6.98 (d, J = 8.4 Hz, 2H), 7.15 (d, J = 8.4 Hz, 2H). ^{13}C-NMR (100 MHz, $CDCl_3$): δ 26.09, 27.66, 29.02, 32.09, 39.58, 54.08, 55.28, 93.92, 114.05, 114.38, 115.86, 128.48, 129.48, 129.89, 130.20, 154.82, 159.89, 162.05, 166.46. MS: *m*/*z* (%) 308.11 (M^+, 100). Anal. calcd for $C_{19}H_{20}N_2O_2$ (308.37): C, 74.00; H, 6.54; N, 9.08. Found: C, 74.17; H, 6.63; N, 9.00.

*5.1.1.5. 4-(4-Fluoro-phenyl)-2-methoxy-6,7,8,9-tetrahydro-5H-cyclohepta[b]pyridine-3-carbonitrile (**3e**).* Colorless microcrystals from *n*-butanol; yield 1.78 g (60%); mp 235–237 °C; IR: ν_{max}/cm^{-1} 2223 (C≡N), 1560 (C=N). ^{1}H-NMR (400 MHz, $CDCl_3$): δ 1.49–1.88 (m, 6H), 2.52 (t, J = 5.6 Hz, 2H), 3.04 (t, J = 5.6 Hz, 2H), 4.05 (s, 3H), 7.14–7.26 (m, 4H). ^{13}C-NMR (100 MHz, $CDCl_3$): δ 26.03, 27.59, 29.04, 32.03, 39.57, 54.17, 93.80, 115.50, 115.94, 129.33, 130.33, 130.41, 132.23, 132.27, 153.87, 162.02, 164.14, 166.79. MS: *m*/*z* (%) 296.10 (M^+, 68), 295.03 (100). Anal. calcd for $C_{18}H_{17}FN_2O$ (296.34): C, 72.95; H, 5.78; N, 9.45. Found: C, 72.80; H, 5.89; N, 9.60.

*5.1.1.6. 4-(3-Chloro-phenyl)-2-methoxy-6,7,8,9-tetrahydro-5H-cyclohepta[b]pyridine-3-carbonitrile (**3f**).* Colorless microcrystals from *n*-butanol; yield 1.88 g (60%); mp 174–176 °C; IR: ν_{max}/cm^{-1} 2219 (C≡N), 1633 (C=N). ^{1}H-NMR (400 MHz, $CDCl_3$): δ 1.49–1.88 (m, 6H), 2.52 (t, J = 5.6 Hz, 2H), 3.04 (t, J = 5.6 Hz,

2H), 4.05 (s, 3H), 7.11 (d, J = 10 Hz, 1H), 7.21 (s, 1H), 7.39–7.44 (m, 2H). ^{13}C-NMR (100 MHz, $CDCl_3$): δ 26.01, 27.56, 29.13, 31.99, 39.57, 54.22, 93.52, 115.22, 126.69, 128.47, 129.03, 129.11, 130.06, 134.62, 138.05, 153.23, 161.99, 166.95. MS: m/z (%) 312.04 (M^+, 59), 311.01 (100). Anal. calcd for $C_{18}H_{17}ClN_2O$ (312.79): C, 69.12; H, 5.48; N, 8.96. Found: C, 69.00; H, 5.30; N, 9.10.

*5.1.1.7. 4-(4-Chloro-phenyl)-2-methoxy-6,7,8,9-tetrahydro-5H-cyclohepta[b]pyridine-3-carbonitrile (**3g**).* Colorless microcrystals from *n*-butanol; yield 1.94 g (62%); mp 229–231 °C; IR: ν_{max}/cm^{-1} 2221 (C≡N), 1557 (C=N). ^{1}H-NMR (400 MHz, $CDCl_3$): δ 1.48–1.88 (m, 6H), 2.52 (t, J = 5.6 Hz, 2H), 3.04 (t, J = 5.8 Hz, 2H), 4.05 (s, 3H), 7.16 (d, J = 8.4 Hz, 2H), 7.44 (d, J = 8.4 Hz, 2H). ^{13}C-NMR (100 MHz, $CDCl_3$): δ 26.02, 27.58, 29.07, 32.01, 39.57, 54.20, 93.57, 115.41, 129.00, 129.16, 129.87, 134.71, 135.04, 153.62, 162.03, 166.90. MS: m/z (%) 312.11 (M^+, 79), 311.06 (100). Anal. calcd for $C_{18}H_{17}ClN_2O$ (312.79): C, 69.12; H, 5.48; N, 8.96. Found: C, 69.30; H, 5.59; N, 8.90.

*5.1.1.8. 4-(3-Bromo-phenyl)-2-methoxy-6,7,8,9-tetrahydro-5H-cyclohepta[b]pyridine-3-carbonitrile (**3h**).* Colorless microcrystals from *n*-butanol; yield 2.22 g (62%); mp 167–168 °C; IR: ν_{max}/cm^{-1} 2221 (C≡N), 1635 (C=N). ^{1}H-NMR (400 MHz, $CDCl_3$): δ 1.51–1.88 (m, 6H), 2.52 (t, J = 5.6 Hz, 2H), 3.04 (t, J = 5.4 Hz, 2H), 4.05 (s, 3H), 7.16 (d, J = 8.8 Hz, 1H), 7.34–7.38 (m, 2H), 7.57 (d, J = 8.8 Hz, 1H). ^{13}C-NMR (100 MHz, $CDCl_3$): δ 26.01, 27.54, 29.14, 31.99, 39.57, 54.22, 93.54, 115.22, 122.68, 127.13, 129.10, 130.28, 131.30, 131.96, 138.30, 153.12, 162.00, 166.94. MS: m/z (%) 356.94 (M^+, 100). Anal. calcd for $C_{18}H_{17}BrN_2O$ (357.24): C, 60.52; H, 4.80; N, 7.84. Found: C, 60.74; H, 4.63; N, 7.76.

*5.1.1.9. 4-(4-Bromo-phenyl)-2-methoxy-6,7,8,9-tetrahydro-5H-cyclohepta[b]pyridine-3-carbonitrile (**3i**).* Colorless microcrystals from *n*-butanol; yield 2.29 g (64%); mp 235–237 °C; IR: ν_{max}/cm^{-1} 2222 (C≡N), 1557 (C=N). ^{1}H-NMR (400 MHz, $CDCl_3$): δ 1.48–1.88 (m, 6H), 2.52 (t, J = 5.6 Hz, 2H), 3.04 (t, J = 5.8 Hz, 2H), 4.05 (s, 3H), 7.09 (d, J = 8.8 Hz, 2H), 7.60 (d, J = 8.8 Hz, 2H). ^{13}C-NMR (100 MHz, $CDCl_3$): δ 26.02, 27.58, 29.08, 32.01, 39.56, 54.21, 93.49, 115.39, 123.27, 129.08, 130.13, 131.95, 135.19, 153.61, 162.03, 166.92. MS: m/z (%) 356.93 (M^+, 100). Anal. calcd for $C_{18}H_{17}BrN_2O$ (357.24): C, 60.52; H, 4.80; N, 7.84. Found: C, 60.41; H, 4.93; N, 7.96.

*5.1.1.10. 4-(1H-Indol-3-yl)-2-methoxy-6,7,8,9-tetrahydro-5H-cyclohepta[b]pyridine-3-carbonitrile (**3j**).* Colorless microcrystals from *n*-butanol; yield 2.00 g (63%); mp 244–246 °C; IR: ν_{max}/cm^{-1} 3438 (NH), 2217 (C≡N), 1635 (C=N). ^{1}H-NMR (400 MHz, $CDCl_3$): δ 1.38–1.84 (m, 6H), 2.66 (t, J = 3.6 Hz, 2H), 3.01–3.13 (m, 2H), 4.07 (s, 3H), 7.13 (t, J = 7.2 Hz, 1H), 7.24–7.34 (m, 3H), 7.44 (d, J = 7.6 Hz, 1H), 8.48 (s, 1H). ^{13}C-NMR (100 MHz, $CDCl_3$): δ 26.09, 27.90, 29.49, 32.21, 39.81, 54.06, 94.86, 111.58, 112.13, 116.42, 119.56, 120.59, 122.78, 124.47, 126.39, 130.96, 135.82, 148.44, 162.39, 166.13. MS: m/z (%) 317.24 (M^+, 100). Anal. calcd for $C_{20}H_{19}N_3O$ (317.38): C, 75.69; H, 6.03; N, 13.24. Found: C, 75.51; H, 6.20; N, 13.30.

*5.1.1.11. 2-Methoxy-4-(1-methyl-1H-indol-3-yl)-5,6,7,8-tetrahydro-quinoline-3-carbonitrile (**3k**).* Yellow microcrystals from ethanol; yield 1.94 g (61%); mp 214–216 °C; IR: ν_{max}/cm^{-1} 2215 (C≡N), 1632 (C=N). ^{1}H-NMR (500 MHz, $CDCl_3$): δ 1.51–2.94 (m, 8H), 3.81 (s, 3H), 4.04 (s, 3H), 7.09–7.42 (m, 5H). ^{13}C-NMR (125 MHz, $CDCl_3$): δ 22.75, 22.90, 26.90, 33.25, 33.52, 54.17, 95.02, 109.94, 110.02, 116.44, 120.24, 122.39, 125.22, 126.35, 128.89, 137.02, 150.10, 159.76, 162.36. MS: m/z (%) 317.16 (M^+, 100). Anal. calcd for $C_{20}H_{19}N_3O$ (317.38): C, 75.69; H, 6.03; N, 13.24. Found: C, 75.84; H, 6.19; N, 13.15.

*5.1.1.12. 2-Methoxy-4-(1-methyl-1H-indol-3-yl)-6,7,8,9-tetrahydro-5H-cyclohepta[b]pyridine-3-carbonitrile (**3l**).* Yellow microcrystals from *n*-butanol; yield 2.09 g (63%); mp 217–219 °C; IR: ν_{max}/cm^{-1} 2221 (C≡N), 1614 (C=N). ^{1}H-NMR (400 MHz, $CDCl_3$): δ 1.59–1.85 (m, 6H), 2.67–2.73 (m, 2H), 3.00–3.13 (m, 2H), 3.87 (s, 3H), 4.06 (s, 3H), 7.13–7.17 (m, 2H), 7.26–7.30 (m, 2H), 7.38 (d, J = 8.8 Hz, 1H). ^{13}C-NMR (100 MHz, $CDCl_3$): δ 26.10, 27.94, 29.49, 32.22, 33.14, 39.83, 54.03, 94.75, 109.73, 110.46, 116.45, 119.75, 120.18, 122.29, 126.91, 128.94, 130.82, 136.78, 148.43, 162.42, 166.00. MS: m/z (%) 331.24 (M^+, 100). Anal. calcd for $C_{21}H_{21}N_3O$ (331.41): C, 76.11; H, 6.39; N, 12.68. Found: C, 76.00; H, 6.57; N, 12.56.

*5.1.1.13. 4-(1-Ethyl-1H-indol-3-yl)-2-methoxy-5,6,7,8-tetrahydro-quinoline-3-carbonitrile (**3m**).* Colorless microcrystals from ethanol; yield 2.13 g (64%); mp 204–206 °C; IR: ν_{max}/cm^{-1} 2217 (C≡N), 1617 (C=N). ^{1}H-NMR (500 MHz, $CDCl_3$): δ 1.53 (t, J = 7.2 Hz, 3H), 1.73–2.95 (m, 8H), 4.04 (s, 3H), 4.22 (q, J = 7.3 Hz, 2H), 7.10–7.41 (m, 5H). ^{13}C-NMR (125 MHz, $CDCl_3$): δ 15.57, 22.77, 22.93, 26.92, 33.52, 41.43, 54.16, 95.02, 110.03, 110.10, 116.22, 120.20, 120.38, 122.23, 125.20, 126.52, 127.38, 136.10, 150.27, 159.71, 162.38. MS: m/z (%) 331.11 (M^+, 100). Anal. calcd for $C_{21}H_{21}N_3O$ (331.41): C, 76.11; H, 6.39; N, 12.68. Found: C, 76.30; H, 6.29; N, 12.76.

*5.1.1.14. 4-(1-Ethyl-1H-indol-3-yl)-2-methoxy-6,7,8,9-tetrahydro-5H-cyclohepta[b]pyridine-3-carbonitrile (**3n**).* Colorless microcrystals from *n*-butanol; yield 2.25 g (65%); mp 192–194 °C; IR: ν_{max}/cm^{-1} 2221 (C≡N),1560 (C=N). ^{1}H-NMR (400 MHz, $CDCl_3$): δ 1.52 (t, J = 7.2 Hz, 3H), 1.60–1.85 (m, 6H), 2.68–2.71 (m, 2H), 2.99–3.12 (m, 2H), 4.06 (s, 3H), 4.22 (q, J = 7.7 Hz, 2H), 7.12–7.16 (m, 1H), 7.25–7.31 (m, 3H), 7.40 (d, J = 8.4 Hz, 1H). ^{13}C-NMR (100 MHz, $CDCl_3$): δ 15.45, 26.11, 27.96, 29.53, 32.22, 39.84, 41.30, 54.03, 94.77, 109.81, 110.53, 116.44, 119.88, 120.12, 122.12, 127.07, 127.46, 130.77, 135.84, 148.60, 162.43, 165.95. MS: m/z (%) 345.23 (M^+, 100). Anal. calcd for $C_{22}H_{23}N_3O$ (345.44): C, 76.49; H, 6.71; N, 12.16. Found: C, 76.70; H, 6.63; N, 12.06.

*5.1.1.15. 2-Methoxy-4-naphthalen-1-yl-6,7,8,9-tetrahydro-5H-cyclohepta[b]pyridine-3-carbonitrile (**3o**).* Colorless microcrystals from *n*-butanol; yield 2.20 g (67%); mp 182–184 °C; IR: ν_{max}/cm^{-1} 2223 (C≡N), 1633 (C=N). ^{1}H-NMR (400 MHz, $CDCl_3$): δ 1.25–1.80 (m, 6H), 2.31 (t, J = 5.6 Hz, 2H), 3.08 (t, J = 7.6 Hz, 2H), 4.09 (s, 3H), 7.26–7.58 (m, 5H), 7.91 (t, J = 8.2 Hz, 2H). ^{13}C-NMR (100 MHz, $CDCl_3$): δ 26.09, 27.47, 29.40, 32.09, 39.70, 54.17, 94.73, 115.19, 124.89, 125.32, 126.30, 126.33, 126.75, 128.57, 129.24, 130.45, 130.84, 133.48, 133.98, 153.76, 162.09, 166.45. MS: m/z (%) 328.06 (M^+, 100). Anal. calcd for $C_{22}H_{20}N_2O$ (328.41): C, 80.46; H, 6.14; N, 8.53. Found: C, 80.60; H, 6.03; N, 8.48.

*5.1.1.16. 2-Amino-8a-methoxy-4-phenyl-4a,5,6,7,8,8a-hexahydro-4H-chromene-3-carbonitrile (**4a**).* Colorless microcrystals from ethanol; yield 1.54 g (54%); mp 188–190 °C; IR: ν_{max}/cm^{-1} 3449, 3348 (NH_2), 2187 (C≡N). ^{1}H-NMR (400 MHz, $CDCl_3$):

δ 1.07–1.87 (m, 8H), 2.30–2.39 (m, 1H), 3.29 (br. s, 1H), 3.32 (s, 3H), 4.36 (s, 2H), 7.19–7.49 (m, 5H). ^{13}C-NMR (100 MHz, $CDCl_3$): δ 22.34, 25.06, 26.50, 30.86, 40.80, 47.13, 48.65, 62.03, 102.76, 120.81, 127.10, 128.09, 128.48, 128.69, 128.90, 141.36, 160.69. MS: *m*/*z* (%) 284.10 (M^+, 4.6), 112.02 (100). Anal. calcd for $C_{17}H_{20}N_2O_2$ (284.35): C, 71.81; H, 7.09; N, 9.85. Found: C, 71.99; H, 7.25; N, 9.77.

*5.1.1.17. 2-Amino-8a-methoxy-4-p-tolyl-4a,5,6,7,8,8a-hexahydro-4H-chromene-3-carbonitrile (**4b**).* Pale yellow microcrystals from ethanol; yield 1.65 g (55%); mp 201–203 °C; IR: ν_{max}/cm^{-1} 3449, 3348 (NH_2), 2184 (C≡N). ^{1}H-NMR (400 MHz, $CDCl_3$): δ 1.09–1.89 (m, 8H), 2.16 (d, J = 11.2 Hz, 1H), 2.34 (s, 3H), 3.24 (br. s, 1H), 3.32 (s, 3H), 4.40 (s, 2H), 7.07–7.52 (m, 4H). ^{13}C-NMR (100 MHz, $CDCl_3$): δ 21.09, 22.36, 25.09, 26.52, 30.87, 40.35, 47.12, 48.63, 62.15, 102.76, 120.94, 128.42, 129.20, 136.55, 138.27, 160.64. MS: *m*/*z* (%) 298.10 (M^+, 14), 112.03 (100). Anal. calcd for $C_{18}H_{22}N_2O_2$ (298.38): C, 72.46; H, 7.43; N, 9.39. Found: C, 72.30; H, 7.58; N, 9.20.

*5.1.1.18. 2-Amino-8a-methoxy-4-(4-methoxy-phenyl)-4a,5,6,7,8,8a-hexahydro-4H-chromene-3-carbonitrile (**4c**).* Yellow microcrystals from ethanol; yield 1.89 g (60%); mp 203–204 °C; IR: ν_{max}/cm^{-1} 3446, 3348 (NH_2), 2183 (C≡N). ^{1}H-NMR (500 MHz, $CDCl_3$): 1.05–1.67 (m, 8H), 2.28 (d, J = 10.5 Hz, 1H), 3.23 (d, J = 10.5 Hz, 1H), 3.30 (s, 3H), 3.78 (s, 3H), 4.37 (s, 2H), 6.83 (d, J = 8.6 Hz, 2H), 7.09 (d, J = 8.6 Hz, 2H). ^{13}C-NMR (125 MHz, $CDCl_3$): δ 22.46, 25.18, 26.59, 30.94, 40.03, 47.30, 48.74, 55.28, 62.20, 102.87, 113.98, 121.15, 129.56, 133.42, 158.67, 160.77. MS: *m*/*z* (%) 314.25 (M^+, 15), 112.12 (100). Anal. calcd for $C_{18}H_{22}N_2O_3$ (314.38): C, 68.77; H, 7.05; N, 8.91. Found: C, 68.60; H, 7.18; N, 8.80.

*5.1.1.19. 2-Amino-4-(4-fluoro-phenyl)-8a-methoxy-4a,5,6,7,8,8a-hexahydro-4H-chromene-3-carbonitrile (**4d**).* Pale yellow microcrystals from ethanol; yield 1.88 g (62%); mp 208–210 °C; IR: ν_{max}/cm^{-1} 3442, 3338, (NH_2), 2186 (C≡N). ^{1}H-NMR (500 MHz, $CDCl_3$): 1.07–1.65 (m, 8H), 2.29 (d, J = 11.4 Hz, 1H), 3.31 (br s, 4H), 4.38 (d, J = 10.5 Hz, 2H), 6.90–7.30 (m, 4H). ^{13}C-NMR (125 MHz, $CDCl_3$): δ 22.41, 25.12, 26.55, 30.92, 40.24, 47.33, 48.77, 61.68, 102.84, 115.36, 115.54, 115.93, 116.10, 120.91, 130.06, 137.18, 160.91. MS: *m*/*z* (%) 302.07 (M^+, 38), 112.05 (100). Anal. calcd for $C_{17}H_{19}FN_2O_2$ (302.34): C, 67.53; H, 6.33; N, 9.27. Found: C, 67.40; H, 6.49; N, 9.17.

*5.1.1.20. 2-Amino-4-(4-bromo-phenyl)-8a-methoxy-4a,5,6,7,8,8a-hexahydro-4H-chromene-3-carbonitrile (**4e**).* Yellow microcrystals from ethanol; yield 2.00 g (55%); mp 205–207 °C; IR: ν_{max}/cm^{-1} 3448, 3319 (NH_2), 2188 (C≡N). ^{1}H-NMR (400 MHz, $CDCl_3$): 1.05–1.65 (m, 8H), 2.30 (d, J = 11.4 Hz, 1H), 3.27 (d, J = 10.8 Hz, 1H), 3.30 (s, 3H), 4.45 (s, 2H), 7.06 (d, J = 8.4 Hz, 2H), 7.42 (d, J = 8.4 Hz, 2H). ^{13}C-NMR (100 MHz, $CDCl_3$): δ 22.28, 25.01, 26.44, 30.81, 40.43, 47.09, 48.70, 61.21, 102.73, 120.68, 120.89, 130.29, 131.64, 140.56, 160.90. MS: *m*/*z* (%) 363.16 (M^+, 6), 112.08 (100). Anal. calcd for $C_{17}H_{19}BrN_2O_2$ (363.25): C, 56.21; H, 5.27; N, 7.71. Found: C, 56.40; H, 5.19; N, 7.87.

5.2. Vasodilation activity screening

Vasodilation properties were assessed using well documented techniques[19–21] such that the effects of the newly synthesized pyridine-3-carbonitriles (**3a–o**) and chromene-3-carbonitrile (**4a–e**) were determined on isolated thoracic aortic rings of male Wister rats (250–350 g). Further details are available in the ESI.†

5.3. *In vitro* antitumor screening

Compounds **3a–o** and **4a–e** were screened against two human cancer cell lines for anti-tumor activity using a cell based approach. The cell line MCF-7 (breast cancer cell line) was obtained from Tenovus centre for cancer research (Cardiff, UK), MDA-MB 231 (epithelial, human breast cancer cell line) was purchased from the European collection of cell cultures (ECACC). The cell culture medium EMEM, fetal bovine serum (FBS), L-glutamine (200 mM), non-essential amino acid (NEAA) [10X], and trypsin EDTA were purchased from Lonza (UK). The cell culture medium RPMI 1640 (with L-glutamine), DMEM (without L-glutamine), DMEM (low glucose, with glutamax), and dimethyl sulfoxide (DMSO) were purchased from Fisher scientific (UK).

3-(4,5-Dimethylthiazol-2-yl)-2,5-diphenyltetrazolium bromide salt was purchased from Sigma-Aldrich (UK).

The cell culture method and MTT cell viability assay used is briefly displayed in ESI.†

5.4. Cell cycle analysis and apoptosis detection

The cell cycle analysis and apoptosis investigations were carried out by flow cytometry.[40] MCF-7 cells were seeded at 8×10^4 and incubated at 37 °C, 5% CO_2 overnight. After treatment with the tested compound, for 24 h, cell pellets were collected and centrifuged (300*g*, 5 min). For cell cycle analysis, cell pellets were fixed with 70% ethanol on ice for 15 min and collected again. The collected pellets were incubated with propidium iodide (PI) staining solution (50 mg mL^{-1} PI, 0.1 mg mL^{-1} RNaseA, 0.05% Triton X-100) at room temperature for 1 hand analyzed by Gallios flow cytometer (Beckman Coulter, Brea, CA, USA). Apoptosis detection was performed by FITC Annexin V/PI commercial kit (Becton Dickenson, Franklin Lakes, NJ, USA) following the manufacture protocol. The samples were analyzed by fluorescence-activated cell sorting (FACS) with a Gallios flow cytometer (Beckman Coulter, Brea, CA, USA) within 1 h after staining. Data were analyzed using Kaluzav 1.2 (Beckman Coulter).

5.5. Caspase-3 activation assay

The activity of caspase-3 was determined using MaxDiscovery™ caspase-3 colorimetric detection kit, Bioo Scientific Corporation (BIOO), USA. Briefly, MCF-7 cells (5×10^5 cells per well) in a 6-well plate were treated with IC_{50} concentrations of compound **3d** for 24 h. The cell culture medium was gently removed from the control and the treated culture wells, and then the cells were lysed by adding cell lysis buffer (1000 μL) to each culture well. The plate was gently shaken for 10 min to facilitate cell lysis and sample homogenization. Caspase-3 substrate (100 μL) was diluted into 10 mL of reaction buffer. In the reaction microplate, 100 μL caspase-3 reaction buffer was added to each well, followed by 100 μL of cell lysate. The absorbance was measured

using a plate reader for the increase in absorbance at 405 nm in 30 min. Caspase-3 activity was expressed as the change of the activity in treated cancer cells compared to the untreated controls.[41,42]

5.6. Molecular docking study

The docking studies were performed using Molecular Operating Environment (MOE-Dock) software version 2014.0901.[37,38] The co-crystallized structure of caspase-3 (PDB code: 2J30)[39] was downloaded from the RCSB Protein Data Bank. All minimizations for the structure were performed with MOE until an RMSD gradient of 0.05 kcal mol^{-1} $Å^{-1}$ with MMFF94x force field and the partial charges were automatically detected. Preparation of caspase-3 kinase structure was achieved using Protonate 3D protocol in MOE with the default options. The docking protocol was achieved using London dG scoring function and Triangle Matcher placement method.

Conflicts of interest

The authors declare no conflicts of interest.

References

1 L. Hu, L. Li, Q. Chang, S. Fu, J. Qin, Z. Chen, X. Li, Q. Liu, G. Hu and Q. Li, Discovery of Novel Pyrazolo[3,4-*b*] pyridine Derivatives with Dual Activities of Vascular Remodeling Inhibition and Vasodilation for the Treatment of Pulmonary Arterial Hypertension, *J. Med. Chem.*, 2020, **63**, 11215–11234.

2 S. Estrada-Soto, M. E. González-Trujano, P. Rendón-Vallejo, L. Arias-Durán, G. Avila-Villarreal and R. Villalobos-Molina, Antihypertensive and vasorelaxant mode of action of the ethanol-soluble extract from *Tagetes lucida* Cav. aerial parts and its main bioactive metabolites, *J. Ethnopharmacol.*, 2021, **266**, 113399.

3 L. Li, W. Zhang, F. Lin, X. Lu, W. Chen, X. Li, X. Zhou, R. Su, L. Wang, Z. Zheng and S. Li, Synthesis and biological evaluation of pyrazolo[3,4-*b*]pyridine-3-yl pyrimidine derivatives as sGC stimulators for the treatment of pulmonary hypertension, *Eur. J. Med. Chem.*, 2019, **173**, 107–116.

4 J. Ferlay, M. Laversanne, M. Ervik, F. Lam, M. Colombet, L. Mery, M. Pineros, A. Znaor, I. Soerjomataram and F. Bray, *Global Cancer Observatory: Cancer Today*, International Agency for Research on Cancer, Lyon, 2020.

5 J. P. Aboumsallem, J. Moslehi and R. A. de Boer, Reverse Cardio-Oncology: Cancer Development in Patients with Cardiovascular Disease, *J. Am. Heart Assoc.*, 2020, **9**, e013754.

6 T. Stocks, M. Van Hemelrijck, J. Manjer, T. Bjorge, H. Ulmer, G. Hallmans, B. Lindkvist, R. Selmer, G. Nagel, S. Tretli, H. Concin, A. Engeland, H. Jonsson and P. Stattin, Blood pressure and risk of cancer incidence and mortality in the Metabolic Syndrome and Cancer Project, *Hypertension*, 2012, **59**, 802–810.

7 T. Hasin, Z. Iakobishvili and G. Weisz, Associated risk of malignancy in patients with cardiovascular disease: evidence and possible mechanism, *Am. J. Med.*, 2017, **130**, 780–785.

8 J. J. Moslehi, Cardiovascular toxic effects of targeted cancer therapies, *N. Engl. J. Med.*, 2016, **375**, 1457–1467.

9 A. Seretis, S. Cividini, G. Markozannes, X. Tseretopoulou, D. S. Lopez, E. E. Ntzani and K. K. Tsilidis, Association between blood pressure and risk of cancer development: a systematic review and meta-analysis of observational studies, *Sci. Rep.*, 2019, **9**, 8565.

10 H. Han, W. Guo, W. Shi, Y. Yu, Y. Zhang, X. Ye and J. He, Hypertension and breast cancer risk: a systematic review and meta-analysis, *Sci. Rep.*, 2017, **7**, 44877.

11 W. C. Meijers and R. A. de Boer, Common risk factors for heart failure and cancer, *Cardiovasc. Res.*, 2019, **115**, 844–853.

12 J. S. Coviello, Cardiovascular and cancer risk: the role of cardio-oncology, *J. Adv. Pract. Oncol.*, 2018, **9**, 160–176.

13 M. Zakaria Stiti, M. Belghobsi, T. Habila, E. Goffin, P. d Tullio, B. Pirotte, G. Faury and S. Khelili, Synthesis and vasodilator activity of new 1,4-dihyropyridines bearing sulfonylurea, urea and thiourea moieties, *Chem. Pap.*, 2020, **74**, 915–928.

14 T. Nakai, N. R. Perl, T. C. Barden, A. Carvalho, A. Fretzen, P. Germano, G. Y. Im, H. Jin, C. Kim, T. W. Lee, L. Long, J. Moore, J. M. Rohde, R. Sarno, C. Segal, E. O. Solberg, J. Tobin, D. P. Zimmer and M. G. Currie, Discovery of IWP-051, a novel orally bioavailable sGC stimulator with once-daily dosing potential in humans, *ACS Med. Chem. Lett.*, 2016, **7**, 465–469.

15 G. S. Masaret, Synthesis, Docking and Antihypertensive Activity of Pyridone Derivatives, *ChemistrySelect*, 2020, **5**, 13995–14003.

16 A. S. Mehanna and J. Y. Kim, Design, synthesis, and biological testing of thiosalicylamides as a novel class of calcium channel blockers, *Bioorg. Med. Chem.*, 2005, **13**, 4323–4331.

17 F. Hernández, A. Sánchez, P. Rendón-Vallejo, C. Millán-Pacheco, Y. Alcaraz, F. Delgado, M. A. Vázquez and S. Estrada-Soto, Synthesis, *ex vivo* and *in silico* studies of 3-cyano-2-pyridone derivatives with vasorelaxant activity, *Eur. J. Med. Chem.*, 2013, **70**, 669–676.

18 A. S. Girgis, A. Kalmouch and M. Ellithey, Synthesis of novel vasodilatory active nicotinate esters with amino acid function, *Bioorg. Med. Chem.*, 2006, **14**, 8488–8494.

19 Z. M. Nofal, A. M. Srour, W. I. El-Eraky, D. O. Saleh and A. S. Girgis, Rational design, synthesis and QSAR study of vasorelaxant active 3-pyridinecarbonitriles incorporating 1H-benzimidazol-2-yl function, *Eur. J. Med. Chem.*, 2013, **63**, 14–21.

20 A. M. Srour, S. S. Abd El-Karim, D. O. Saleh, W. I. El-Eraky and Z. M. Nofal, Rational design, synthesis and 2D-QSAR study of novel vasorelaxant active benzofuran-pyridine hybrids, *Bioorg. Med. Chem. Lett.*, 2016, **26**, 2557–2561.

21 N. M. Khalifa, A. M. Srour, S. S. AbdEl-Karim, D. O. Saleh and M. A. Al-Omar, Synthesis and 2D-QSAR Study of Active Benzofuran-Based Vasodilators, *Molecules*, 2017, **22**, 1820.

22 A. M. Srour, D. H. Dawood and D. O. Saleh, Synthesis, 3D-pharmacophore modelling and 2D-QSAR study of new pyridine-3-carbonitriles as vasorelaxant active agents, *New J. Chem.*, 2021, **45**, 7731–7740.

23 S. Singh, K. Agarwal, H. Iqbal, P. Yadav, D. Yadav, D. Chanda, S. Tandon, F. Khan, A. K. Gupta and A. Gupta, Synthesis and evaluation of substituted 8,8-dimethyl-8*H*-pyrano[2,3-*f*]chromen-2-one derivatives as vasorelaxing agents, *Bioorg. Med. Chem. Lett.*, 2020, **30**, 126759.

24 T. Yamanaka, M. Yasumoto, T. Nakajima and O. Yaoka, *Chem. Abstr.*, 1993, **118**, 169097, Jpn. Kokai Tokkyo Koho JP 04,282,353 (92,282,353) (Cl. C07C239/20), 7 Oct. 1992.

25 M. Baumgarth, R. Gericke, I. Lues, J. De Peyer and R. Bergmann, *Chem. Abstr.*, 1989, **111**, 97213, Eur. Pat. Appl. EP 308,792 (Cl. C07D491/04), 29 Mar. 1989.

26 J. M. Evans, G. Stemp and F. Cassidy, *Chem. Abstr.*, 1987, **106**, 213921, Eur. Pat. Appl. EP 205,292 (Cl. C07D491/04), 17 Dec. 1986.

27 A. S. Girgis, N. S. M. Ismail and H. Farag, Facile synthesis, vasorelaxant properties and molecular modeling studies of 2-amino-8*a*-methoxy-4*H*-pyrano[3,2-c]pyridine-3-carbonitriles, *Eur. J. Med. Chem.*, 2011, **46**, 2397–2407.

28 A. Malki, M. Mohsen, H. Aziz, O. Rizk, O. Shaaban, M. El-Sayed, Z. A. Sherif and H. Ashour, New 3-Cyano-2-Substituted Pyridines Induce Apoptosis in MCF 7 Breast Cancer Cells, *Molecules*, 2016, **21**, 230.

29 K. M. Abouzid, G. H. Al-Ansary and A. M. El-Naggar, Eco-friendly synthesis of novel cyanopyridine derivatives and their anticancer and PIM-1 kinase inhibitory activities, *Eur. J. Med. Chem.*, 2017, **134**, 357–365.

30 R. Sabour, M. F. Harras, O. M. Al Kamaly and N. Altwaijry, Discovery of Novel 3-Cyanopyridines as Survivin Modulators and Apoptosis Inducers, *Molecules*, 2020, **25**, 4892.

31 G. Gudipudi, S. R. Sagurthi, S. Perugu, G. Achaiah and G. L. David Krupadanam, Rational design and synthesis of novel 2-(substituted-2*H*-chromen-3-yl)-5-aryl-1*H*-imidazole derivatives as an anti-angiogenesis and anti-cancer agent, *RSC Adv.*, 2014, **4**, 56489–56501.

32 H. E. A. Ahmed, M. A. A. El-Nassag, A. H. Hassan, R. M. Okasha, S. Ihmaid, A. M. Fouda, T. H. Afifi, A. Aljuhani and A. M. El-Agrody, Introducing novel potent anticancer agents of 1*H*-benzo[*f*]chromene scaffolds, targeting c-Src kinaseenzyme with MDA-MB-231 cell line anti-invasioneffect, *J. Enzyme Inhib. Med. Chem.*, 2018, **33**, 1074–1088.

33 A. S. Girgis, D. O. Saleh, R. F. George, A. M. Srour, G. G. Pillai, C. S. Panda and A. R. Katritzky, Synthesis, bioassay, and QSAR study of bronchodilatory active 4*H*-pyrano[3,2-*c*]pyridine-3-carbonitriles, *Eur. J. Med. Chem.*, 2015, **89**, 835–843.

34 T. Rudel, Caspase inhibitors in prevention of apoptosis, *Herz*, 1999, **24**, 236–241.

35 P. D. Mace, S. J. Ried and G. S. Salvesen, Chapter seven-caspase enzymology and activation mechanisms, *Methods Enzymol.*, 2014, **544**, 161–178.

36 T. M. Thornton and M. Rincon, Non-Classical P38 Map Kinase Functions: Cell Cycle Checkpoints and Survival, *Int. J. Biol. Sci.*, 2009, **5**, 44–52.

37 A. E. G. E. Amr, E. A. Elsayed, M. A. Al-Omar, H. O. Badr Eldin, E. S. Nossier and M. M. Abdallah, Design, synthesis, anticancer evaluation and molecular modeling of novel estrogen derivatives, *Molecules*, 2019, **24**(3), 416.

38 E. S. Nossier, S. M. El-Hallouty and E. R. Zaki, Synthesis, anticancer evaluation and molecular modeling of some substituted thiazolidinonyl and thiazolyl pyrazole derivatives, *Int. J. Pharm. Sci.*, 2015, **7**, 353–359.

39 B. Feeney, C. Pop, P. Swartz, C. Mattos and A. C. Clark, Role of loop bundle hydrogen bonds in the maturation and activity of (Pro) caspase-3, *Biochemistry*, 2006, **45**(44), 13249–13263.

40 S. Diab, T. Teo, M. Kumarasiri, P. Li, M. Yu, F. Lam, S. K. C. Basnet, M. J. Sykes, H. Albrecht, R. Milne and S. Wang, Discovery of 5-(2-(phenylamino) pyrimidin-4yl) thiazol-2(3*H*)-one derivatives as potent Mnk2 inhibitors: synthesis, SAR analysis and biological evaluation, *ChemMedChem*, 2014, **9**, 962–972.

41 V. Gurtu, S. R. Kain and G. Zhang, Fluorometric and Colorimetric Detection of Caspase Activity Associated with Apoptosis, *Anal. Biochem.*, 1997, **251**, 98–102.

42 N. Dong, X. Liu, T. Zhao, L. Wang, H. Li, S. Zhang, X. Li, X. Bai, Y. Zhang and B. Yang, Apoptosis-inducing effects and growth inhibitory of a novel chalcone, in human hepatic cancer cells and lung cancer cells, *Biomed. Pharmacother.*, 2018, **105**, 195–203.